Activation of the SK potassium channel-calmodulin complex by nanomolar concentrations of terbium

Weiyan Li and Richard W. Aldrich[1]

Section of Neurobiology, Center for Learning and Memory, University of Texas, Austin, TX 78712

Contributed by Richard W. Aldrich, November 25, 2008 (sent for review October 30, 2008)

Small conductance Ca^{2+}-activated K^+ (SK) channels sense intracellular Ca^{2+} concentrations via the associated Ca^{2+}-binding protein calmodulin. Structural and functional studies have revealed essential properties of the interaction between calmodulin and SK channels. However, it is not fully understood how the binding of Ca^{2+} to calmodulin leads to channel opening. Drawing on previous biochemical studies of free calmodulin using lanthanide ions as Ca^{2+} substitutes, we have used the lanthanide ion, Tb^{3+}, as an alternative ligand to study the activation properties of SK channels. We found that SK channels can be fully activated by nanomolar concentrations of Tb^{3+}, indicating an apparent affinity >100-fold higher than Ca^{2+}. Competition experiments show that Tb^{3+} binds to the same sites as Ca^{2+} to activate the channels. Additionally, SK channels activated by Tb^{3+} demonstrate a remarkably slow deactivation process. Comparison of our results with previous biochemical studies suggests that in the intact SK channel complex, the N-lobe of calmodulin provides ligand-binding sites for channel gating, and that its ligand-binding properties are comparable to those of the N-lobe in isolated calmodulin.

lanthanide | EF hand | gating | calcium-activated potassium channel

Small conductance Ca^{2+}-activated K^+ (SK, $K_{Ca}2$) channels sense Ca^{2+} concentrations via the associated Ca^{2+}-binding protein calmodulin (CaM) (1). CaM consists of two globular lobes connected by a flexible linker, referred to as the N-lobe and the C-lobe. Each of the two lobes contains two EF hand motifs that bind Ca^{2+}. Ca^{2+} binding to the EF hands of CaM constitutively associated with channel subunits leads to rapid opening of the SK channel pore (2). Structural and functional studies have provided important insights into the molecular mechanism for the coupling between CaM and SK channels (2). The crystal structure of the intracellular CaM-binding domain (CaMBD) (96 aa) of the SK channel was solved in association with Ca^{2+}-loaded CaM. This structure suggests that the C-lobe of CaM mediates the constitutive interaction with the CaMBD of SK channels. As a result of this interaction, the C-lobe loses its ability to bind Ca^{2+}. The N-lobe sites are loaded with Ca^{2+} in the structure, suggesting that Ca^{2+} activation of SK channels is the result of Ca^{2+} binding to the two EF hands in the N-lobe of CaM (3). Functional studies with CaM mutants are consistent with this idea: Mutations at the N-lobe of CaM that abolish Ca^{2+} binding dramatically affect the Ca^{2+} gating of SK channels, whereas the equivalent mutations at the C-lobe have no effect (4). However, the molecular mechanisms for the CaM-SK coupling emerging from these studies are less than conclusive because of some experimental limitations. The structure only includes a relatively small segment of the SK channel (3); therefore, it is necessary to verify that it correctly depicts the interaction between CaM and full-length SK channels. Also, the interpretation of CaM mutational studies was complicated by the presence of endogenous wild-type CaM in the expression system.

Understanding of the gating mechanisms for ligand-gated ion channels has been facilitated by the use of a collection of chemically related ligands that interact differently with the channels. Such an approach has not been useful in the study of SK channels, however. In contrast to other channel types gated by small organic molecules for which many ligands are often available, SK channels are activated by an ion. Furthermore, SK channels have high selectivity for Ca^{2+} over other divalent ions, making these less useful as alternative ligands (5). However, trivalent lanthanide ions such as terbium (Tb^{3+}) and europium (Eu^{3+}) ions have been frequently used to substitute for Ca^{2+} in biochemical studies of Ca^{2+}-binding proteins such as CaM. Lanthanide ions can bind to the Ca^{2+}-binding sites because of their similar ionic size and coordinating properties as Ca^{2+}. The unique spectroscopic properties of some lanthanide ions allow for optical measurement of ligand binding, which has helped elucidate the affinity and order of Ca^{2+} binding to the four Ca^{2+}-binding sites of CaM (6–9). Given that CaM serves as the Ca^{2+} sensor for SK channels, we have investigated the activation of SK channels by lanthanide ions (mainly Tb^{3+}), with the expectation that they may serve as alternative ligands to Ca^{2+}, and that functional differences between lanthanide and Ca^{2+} ions can enhance the understanding of the gating mechanisms of SK channels. By directly applying Tb^{3+} to heterologously expressed SK channels, we found that like Ca^{2+}, Tb^{3+} can fully activate SK channels. Comparing the functional effects of Ca^{2+} and Tb^{3+} on the activation and deactivation of SK channels provides insights into the coupling mechanism between CaM and SK channels.

Results

Although lanthanide ions including Tb^{3+} have been shown to bind to the Ca^{2+}-binding sites and activate purified CaM protein (8, 10–13), their functional effects on CaM-dependent ion channels have not been studied. We directly applied Tb^{3+} ions to excised patches from *Xenopus* oocytes heterologously expressing SK channels to test their effects on activation.

In previous studies on Ca^{2+}-activated channels including SK channels, Ca^{2+} chelators have been used in internal solutions to control free Ca^{2+} concentrations. However, these chelators have extremely high affinity for Tb^{3+} and other lanthanide ions (stability constants $>10^{15}$ M^{-1}) (14). It is not feasible to achieve the desired Tb^{3+} concentrations in the presence of any of these Ca^{2+} chelators. Additionally, appropriate selective chelators for lanthanide ions at nanomolar to micromolar concentration are not available. We decided to use chelator-free solution (CFS) to test the effect of Tb^{3+}. However, without Ca^{2+} chelators we need to reduce the contaminating Ca^{2+} in our solution (usually a few μM, sufficient to saturate the activation of SK channels). By using columns made of Chelex 100 resin (see *Materials and Methods*), we were able to reproducibly reduce the Ca^{2+} contamination to approximately 300 nM level, as measured with

Author contributions: W.L. and R.W.A. designed research; W.L. performed research; W.L. and R.W.A. analyzed data; W.L. and R.W.A. wrote the paper.

The authors declare no conflict of interest.

[1]To whom correspondence should be addressed at: Section of Neurobiology, Center for Learning and Memory, 1 University Station C7000, University of Texas, Austin, TX, 78712. E-mail: raldrich@mail.utexas.edu.

© 2009 by The National Academy of Sciences of the USA

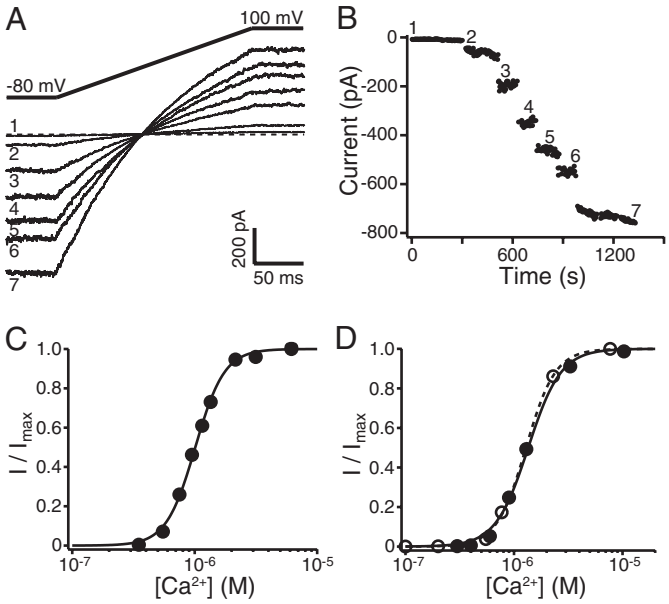

Fig. 1. Activation of SK channels by Ca^{2+}. (*A*) Representative SK current traces elicited by a voltage ramp from −80 to 100 mV at different total Ca^{2+} concentrations ($[Ca^{2+}]$). Currents were recorded from an inside-out patch pulled from an oocyte expressing SK channels. To achieve desired $[Ca^{2+}]$, calculated amounts of Ca^{2+} stock solution were added to the bath (CFS with 350 nM contaminating Ca^{2+}) in a Petri dish before thorough mixing by pipeting. The $[Ca^{2+}]$ (350 nM + added amount) for individual traces are: 1, 0.35 μM; 2, 0.55 μM; 3, 0.75 μM; 4, 0.95 μM; 5, 1.15 μM; 6, 1.35 μM; and 7, 6.15 μM. (*B*) SK current level at −80 mV measured every three seconds while Ca^{2+} was added to the bath. Data points during mixing were noisy and removed from the plot. Numbers correspond to the traces in *A*. (*C*) Mean current level at −80 mV at each $[Ca^{2+}]$ normalized to the maximal value at 6.15 μM and plotted as a function of $[Ca^{2+}]$. Solid line represents fit of the data with the Hill equation (EC_{50} = 1.01 μM, Hill coefficient h = 3.66). (*D*) Ca^{2+} dose-response relationship was measured with both CFS (solid circles) and chelator-containing Ca^{2+} solutions (open circles) in a same patch (see *Materials and Methods*). Fits with Hill equation yield: CFS, EC_{50} = 1.35 μM, h = 2.87 (solid line); with chelators, EC_{50} = 1.29 μM, h = 3.21 (dashed line).

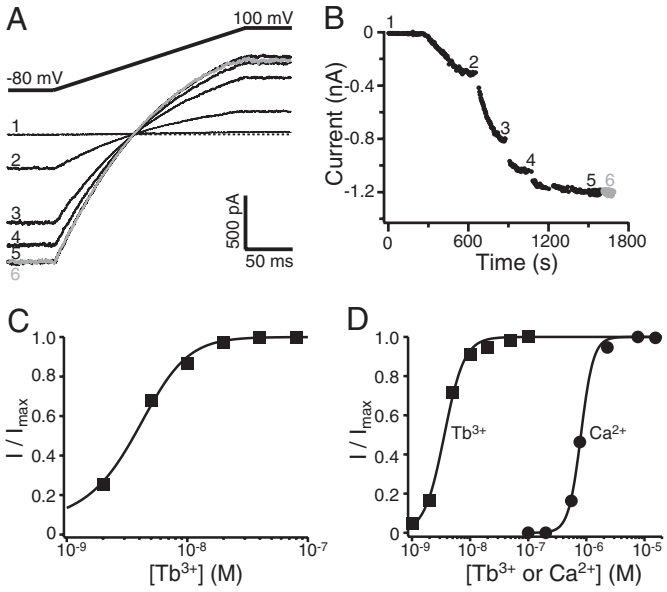

Fig. 2. Activation of SK channels by Tb^{3+}. (*A*) Representative SK current traces elicited by a voltage ramp from −80 to 100 mV at different total Tb^{3+} concentration ($[Tb^{3+}]$). The recording conditions were as in Fig. 1*A*. The bath solution (CFS) contained 300 nM contaminating Ca^{2+}. To achieve desired $[Tb^{3+}]$, appropriate amounts of 1 μM Tb^{3+} stock solution were added to the bath before thorough mixing by pipeting. The $[Tb^{3+}]$ for individual traces are: 1, 0 nM; 2, 2 nM; 3, 5 nM; 4, 10 nM; 5, 80 nM; and 6, 80 nM +10 μM Ca^{2+} (gray trace). (*B*) SK current level at −80 mV measured every three seconds while Tb^{3+} was added to the bath. Data points during mixing were removed from the plot. Numbers correspond to the traces in *A*. (*C*) Mean current levels at −80 mV normalized to the maximal current and plotted as a function of $[Tb^{3+}]$. Solid line represents fit with the Hill equation (EC_{50} = 3.47 nM, h = 1.93). (*D*) Tb^{3+} (solid squares) and Ca^{2+} (solid circles) dose-response relationships measured in a same patch (see *Materials and Methods*). Solid lines are fits with the Hill equation (Tb^{3+}: EC_{50} = 3.60 nM, h = 2.53; Ca^{2+}: EC_{50} = 0.81 μM, h = 4.06).

Fura-2. Tb^{3+} or Ca^{2+} was then added to the decalcified CFS to achieve the desired concentrations.

To verify our approach, we first measured the activation of SK channels by Ca^{2+} using CFS and added Ca^{2+}. Contaminating Ca^{2+} (≈300 nM) alone in CFS did not significantly activate SK channels (Fig. 1*A*, trace 1), but larger SK currents emerged when additional Ca^{2+} was added (Fig. 1*A* traces 2–7 and *B*). Current levels at −80 mV are normalized and plotted as a function of total Ca^{2+} concentration (contaminating + added), which is fitted with the Hill equation $I/I_{max} = 1/(1+(EC_{50}/[Ca^{2+}])^h)$ (Fig. 1*C*). Average results from 11 patches show that Ca^{2+} activates SK channels with a half activation concentration (EC_{50}) of approximately 1.2 μM, and Hill coefficient (h) of approximately 3.7 (Table 1). To compare these results with previous measurements in the presence of Ca^{2+} chelators, in eight of the 11 experiments, we also measured Ca^{2+} dose-response relationships by using chelator-containing Ca^{2+} solutions on the same patches (see *Materials and Methods*). Results from one such experiment are shown in Fig. 1*D*. The dose-response relationships obtained using the two methods are very similar (Table 1), suggesting that the use of CFS provides reliable measurements of the dose-response relationship for SK channel activation, and that the results using CFS are comparable to the measurements using Ca^{2+} chelators. Our measured EC_{50} values for Ca^{2+} activation of SK channels are somewhat different from previous studies (≈0.3–0.5 μM) (1, 4, 15), likely a result of different ways to determine free Ca^{2+} concentrations in the presence of Ca^{2+} chelators. Alternatively, this discrepancy could have resulted from differences in the phosphorylation status of CaM (16).

Activation of SK channels by Tb^{3+} was similarly measured by adding Tb^{3+} to the bath solution. Fig. 2 *A* and *B* shows that

Table 1. Different functional effects of Ca^{2+} and Tb^{3+} on SK channel gating

	Apparent affinity for activation			Deactivation kinetics	
	EC_{50}	Hill coefficient, h	No. of trials	Time constant, τ	# of trials
Ca^{2+} + CFS	1.17 ± 0.24 μM	3.68 ± 0.82	n = 11	51.6 ± 10.6 ms	n = 6
Ca^{2+} + Chelator	1.27 ± 0.24 μM	3.45 ± 0.73	n = 8	78.4 ± 18.5 ms	n = 7
Tb^{3+}	5.17 ± 2.86 nM	1.74 ± 0.47	n = 37	8.28 ± 3.45 s	n = 10

Values are reported as mean ± SD

addition of 2 nM Tb^{3+} was sufficient to activate significant amount of SK channels, although with a slower time course compared with μM range Ca^{2+} (compare Figs. 2*B* and 1*B*). Greater SK currents were activated with increasing Tb^{3+} concentration, until saturation at 40–80 nM total Tb^{3+} (Fig. 2*A* and *B*). The SK currents activated by Tb^{3+} have similar current-voltage relationship to those activated by either Ca^{2+} in CFS (Fig. 1*A*), or Ca^{2+} solutions with chelators (data not shown), and to SK currents in previous studies (for example, 1, 4). As shown by trace 6 (gray) in Fig. 2*A* and the time course in Fig. 2*B* (compare 6 and 5), after saturation of activation with 80 nM total Tb^{3+}, addition of 10 μM Ca^{2+} in the presence of Tb^{3+} did not elicit further SK current, although it slightly reduced the current at positive potentials, presumably because of Ca^{2+} block (5). This result suggests that like Ca^{2+}, Tb^{3+} is a full agonist for SK channels.

The dose-response relationship for Tb^{3+} activation of SK channels shown in Fig. 2*C* is fitted with the Hill equation (EC_{50} = 3.47 nM and h = 1.93). In this fit, the contribution by the contaminating Ca^{2+} ($\approx$300 nM) is ignored. Exactly how the contaminating Ca^{2+} affects the measured Tb^{3+} activation of SK channels depends on the unknown interaction between Ca^{2+} and Tb^{3+} when they both bind to the same channels. However, it is likely that the effect of contaminating Ca^{2+} on the values of EC_{50} and h for Tb^{3+} is small, because the concentration of contaminating Ca^{2+} in CFS is only approximately 1/4 of the measured EC_{50} for Ca^{2+} activation, and it alone usually activates <1% of the SK channels. Regardless of the exact mechanism for the Ca^{2+}-Tb^{3+} interaction, it is evident that approximately 5 nM Tb^{3+} can substitute for approximately 900 nM Ca^{2+} to half-maximally activate the SK channels in the presence of approximately 300 nM contaminating Ca^{2+}. Therefore, Tb^{3+} activates SK channels with >100-fold higher apparent affinity than Ca^{2+}. Based on individual fits of data from 37 patches (neglecting the contribution by contaminating Ca^{2+}), the average results for Tb^{3+} activation of SK channels yielded EC_{50} = 5.17 $\pm$ 2.86 nM, h = 1.74 $\pm$ 0.47. The h values for Tb^{3+} activation are significantly lower compared with values for Ca^{2+} activation of SK channels (Student's *t* test, $P < 0.01$) (Table 1), suggesting less cooperativity in activation by Tb^{3+} than by Ca^{2+}. However, it should be kept in mind that Hill equation is only a simple empirical description of the dose-response relationship. For an SK channel complex with multiple CaMs, each containing multiple binding sites, we cannot make further conclusions about cooperativity without a more thorough understanding of the activation mechanism.

We noticed a rather large variation in EC_{50} and h values for Tb^{3+} activation of SK channels among different patches. The low concentrations of Tb^{3+} used and the absence of chelators in our solutions make our measurements more sensitive to even trace amounts of contamination and inaccuracies in determination of concentration. Other possible reasons for this variation include variable local Tb^{3+} concentrations because of different levels of endogenous chelating molecules and surface charges across patches, and variability in the properties of the SK channel complex related to the phosphorylation status of CaM (16). Occasionally (<10%), we came across EC_{50}s for Tb^{3+} activation that were >3-fold higher than the average value. Those experiments were considered as outliers and excluded from further analysis (Chauvenet's criterion).

To compare Ca^{2+} and Tb^{3+} activation of SK channels more directly, we measured both Ca^{2+} and Tb^{3+} dose-response relationships from the same patches (see *Materials and Methods*). Fig. 2*D* shows the Ca^{2+} and Tb^{3+} dose-response relationships from one such experiment. Average results from five such patches show that Ca^{2+} activates SK channels with EC_{50} = 0.91 $\pm$ 0.21 μM, h = 4.30 $\pm$ 1.51; and for Tb^{3+}, EC_{50} = 3.47 $\pm$ 1.05 nM, h = 2.16 $\pm$ 0.84, confirming that within the same patches Tb^{3+} activates SK channels with >100-fold higher apparent affinity than Ca^{2+}.

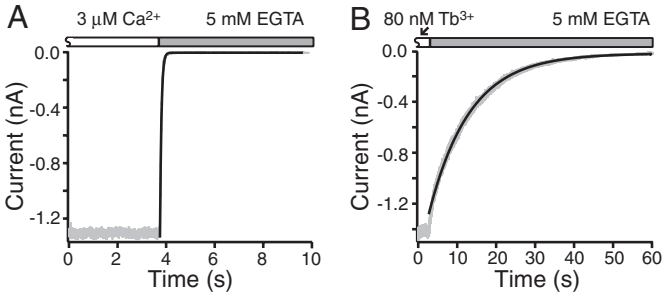

Fig. 3. Deactivation kinetics of SK channels activated by Ca^{2+} or Tb^{3+}. (*A*) After the activation of SK channels by CFS +3 μM Ca^{2+} stabilized, current (gray) at −80 mV was recorded at 100-μs intervals while the recording pipette was quickly moved into a laminar flow of the Ca^{2+}-free solution (5 mM EGTA, see *Materials and Methods*). Time 0 is arbitrarily chosen for illustration purpose in this and the following figures. Dark solid line is a fit with single exponential time course (τ = 58 ms). (*B*) In a different patch, after SK channel activation stabilized in CFS + 80 nM Tb^{3+}, deactivation was measured as in *A*. Dark solid line is a fit with single exponential time course (τ = 10.5 s).

Previous biochemical studies indicated that the dissociation rates for Tb^{3+} from CaM are much slower than Ca^{2+} (17, 18), as would be expected by the difference in affinities (19). To test whether this difference in dissociation is reflected in the kinetics of SK channels, we compared the deactivation of SK channels when Ca^{2+} or Tb^{3+} is removed from CaM. To minimize rebinding of ligand during deactivation, we quickly moved the patch into Ca^{2+}-free solution (5 mM EGTA). As shown in Fig. 3*A*, when SK channels are activated by Ca^{2+} alone, the deactivation process demonstrates a fast decay of current, which can be fitted well by using a single exponential time course with time constants of approximately 50 ms (Table 1). This time constant is comparable with the measured values using an automated fast solution changing system (20). When SK channels are activated by a saturating concentration of Tb^{3+}, the majority of the current decay during deactivation can also be fitted with a single exponential time course (Fig. 3*B*), but with a time constant of approximately 10 s (Table 1). The deactivation process for Tb^{3+}-activated SK channels is therefore >100-fold slower than that for SK channels activated by Ca^{2+}. This difference would be expected from the >100-fold higher apparent affinity under the conditions where the deactivation rate is limited by ligand dissociation, and binding rates for Tb^{3+} and Ca^{2+} are similar. In some experiments, including the one shown in Fig. 3*B*, a small fraction of the current at the beginning of the deactivation follows a faster time course, which is likely because of the presence of the contaminating approximately 300 nM Ca^{2+} in the CFS (see below).

If Tb^{3+} and Ca^{2+} bind to the same sites in CaM associated with SK channels, their binding should be competitive. The large difference in deactivation kinetics allowed us to test directly for competition. For this purpose, we added 10 μM Ca^{2+} to the bath solution in the presence of 80 nM Tb^{3+} after the SK channels were fully activated with Tb^{3+}. When equilibrium was reached after thorough mixing and >3-min incubation, no further SK current was activated by this extra Ca^{2+} (data not shown). However, the deactivation kinetics were very different from when the channels were activated by 80 nM Tb^{3+} alone (compare Figs. 4*A* and 3*B*). Fitting the current decay requires at least two major exponential components, one with a time constant of approximately 1 s, the other approximately 10 s. Average results from five similar experiments indicate that approximately 70% of the SK channels deactivate with the slow time course, whereas approximately 30% deactivate with the fast time course. The

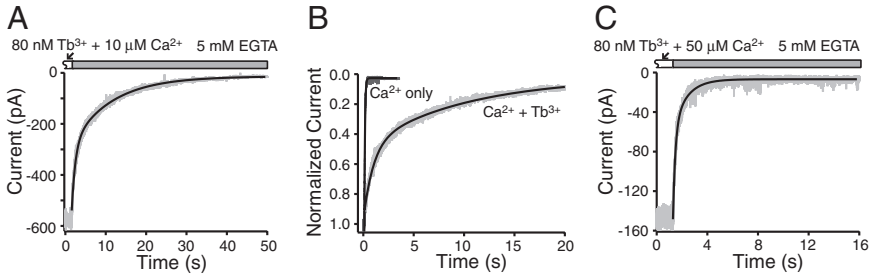

Fig. 4. Effects of the competition between Ca^{2+} and Tb^{3+} on the deactivation kinetics of SK channels. (*A*) Experiment was done as in Fig. 3*B* except that 10 μM Ca^{2+} was added to the bath after 80 nM Tb^{3+}. Bath was mixed thoroughly and incubated for >3 min before the pipette was moved into Ca^{2+}-free solution. Current decay (gray) is fitted with two exponential components (dark solid line) with $\tau_1 = 0.93$ s (49%), $\tau_2 = 9.91$ s (51%). (*B*) With the same patch in *A*, deactivation was measured again after reactivating the channels with chelator-containing solution (15.4 μM free Ca^{2+}). Current trace (*Left*, gray) is plotted with the trace and fit from *A* (*Right*, gray trace and dark solid line) on an expanded time scale after normalized to the current level before deactivation. The new deactivation current trace is fitted with a single exponential time course ($\tau = 65$ ms, dark solid line). Brief downward spikes in this and other traces likely resulted from the activation of stretch-activated channels. They do not affect the exponential fits. (*C*) Deactivation measured after stabilized activation of SK channels by 80 nM Tb^{3+} +50 μM Ca^{2+}. Current decay (gray) is fitted with two exponential time course ($\tau_1 = 0.19$ s, 64%; $\tau_2 = 1.06$ s, 36%; dark solid line).

significant presence of this fast component in deactivation suggests that Ca^{2+} can indeed compete with Tb^{3+} for the same ion-binding sites in CaM. The slower time course is comparable with the deactivation of SK channels activated by Tb^{3+} alone, whereas the fast time course is still much slower than expected for channels activated by Ca^{2+} alone (≈50 ms). To measure the deactivation of SK channels activated by Ca^{2+} alone in the same patches, we reactivated SK channels by using chelator-containing solutions with saturating free Ca^{2+} concentration. Presumably all Tb^{3+} ions in the solution were chelated by Ca^{2+} chelators because of their extremely high affinity, and the channels should be activated only by Ca^{2+}. As expected, deactivation after this treatment shows a fast, single-exponential decay, with time constants close to those for SK channels activated by Ca^{2+} alone in CFS (Fig. 4*B* and Table 1).

From Fig. 4*B*, it is clear that the faster component ($\tau = \approx 1$ s) of the deactivation process for SK channels activated by Tb^{3+} + Ca^{2+} is still slower than the deactivation of SK channels activated by Ca^{2+} alone ($\tau = \approx 50$ ms). The channel deactivation cannot be described by the combination of two components with the measured fast time constant for Ca^{2+} alone and the slow time constant for Tb^{3+} alone, suggesting that Ca^{2+} and Tb^{3+} can collectively activate a single channel and thus producing an intermediate time course in deactivation. Each SK channel has 4 associated CaMs, which together have at least eight functional ion-binding sites for activation (3). SK channels could have many combinations of different numbers of bound Ca^{2+} and Tb^{3+}, potentially resulting in different deactivation kinetics. Fitting the deactivation with exponential time courses does not allow us to distinguish more than three components. The intermediate time constants from the fit of the deactivation likely reflect the combined result of multiple species with different numbers of bound Tb^{3+} and Ca^{2+}. Consistent with the competition between Ca^{2+} and Tb^{3+}, when 50 μM Ca^{2+} was added after 80 nM Tb^{3+}, the slow component was virtually absent from the deactivation process. As shown in Fig. 4*C*, the time course of deactivation can be still fitted with two exponential components, with the longer time constant at approximately 1 s, and the shorter one at approximately 200 ms, which approaches the fast deactivation process with Ca^{2+} alone. We found that the deactivation of SK channels activated by nonsaturating Tb^{3+} concentrations (e.g., 2 nM and 5 nM) demonstrates both a slow ($\tau = \approx 10$ s) and a significant fast ($\tau = \approx 1$ s) component (data not shown), likely reflecting competition between Tb^{3+} and the contaminating Ca^{2+} (≈300 nM) in our solution. We also measured deactivation of SK channels over a range of different concentrations of competing Ca^{2+} (1–20 μM) in the presence of 80 nM Tb^{3+}. Although the deactivation can always be fitted with a fast ($\tau = \approx 1$ s) and a slow ($\tau = \approx 10$ s) component, the relationship between Ca^{2+} concentration and the fraction of each component in the deactivation was too variable across different patches to allow detailed quantitative comparison. It is likely that this variability is partly a result of variable Tb^{3+} apparent affinity among different patches, and partly reflects the inadequacy of using exponential fits with only a few components to characterize a complicated deactivation process. Nevertheless, the trend from these results indicates clearly that increased Ca^{2+} concentration leads to a decrease in the amplitude of the slow component in the deactivation process, as expected for competition between fast unbinding Ca^{2+} and slow unbinding Tb^{3+}.

Discussion

Activation of SK Channels by Nanomolar Tb^{3+}. In the present study, we established conditions where activation of SK channels by lanthanide ions can be directly measured with patch-clamp recording. Our results demonstrate that Tb^{3+} activates SK channels at nanomolar concentrations. We have also tested europium (Eu^{3+}) and lanthanum (La^{3+}) ions, and obtained results qualitatively similar to Tb^{3+} in terms of apparent affinity and kinetics (data not shown). Lanthanide ions such as Tb^{3+} and Eu^{3+} were shown with biochemical assays to bind the Ca^{2+}-binding sites in purified CaM protein with higher affinity than Ca^{2+} (9, 19). The higher affinity was generally attributed to the fact that lanthanide ions are similar in size to Ca^{2+} but carry an extra charge, enhancing the association with the negatively charged EF hands. In particular, lanthanide ions were found to bind very tightly to the N-lobe of CaM (8, 21). With the help of the high quantum yield of the Eu^{3+} ion in D_2O, the binding affinity of Eu^{3+} at the N-lobe was directly measured by using 50 nM purified CaM, yielding K_d of approximately 6–12 nM (19). In our study, we used the activation of SK channels as a reporter to show that, in a functionally complete SK channel complex CaM is indeed effectively activated by a few nanomolar lanthanide ions. Our experiments did not directly measure lanthanide binding to CaM, and the opening of SK channels is unlikely to be linearly correlated to the number of bound ligands. However, regardless of the exact number of lanthanide ions required for channel opening, our measurement is in excellent agreement with the earlier estimates of the high-affinity binding of lanthanide ions to CaM (19).

In contrast to the strong biochemical interest in using lanthanide ions as a tool to study Ca^{2+} binding, it has been rarely tested whether binding of lanthanide ions in CaM is functionally equivalent to the binding of Ca^{2+} in a complete biological

context. Our data demonstrate that lanthanide ions can activate SK channels through binding to the associated CaM. Competition between Ca^{2+} and Tb^{3+}, as demonstrated in the measurements of channel deactivation (Fig. 4), established that lanthanide ions bind to the same sites as Ca^{2+} to activate SK channels. Both Tb^{3+} and Ca^{2+} can fully activate SK channels, and the appearance of SK currents activated by Tb^{3+} is similar to those activated by Ca^{2+} (Figs. 1 and 2). Additionally, our results indicate that Tb^{3+} and Ca^{2+} can collaboratively activate a single channel (Fig. 4*B*). All of the above evidence collectively suggests that lanthanide ions induce similar conformational changes in CaM as does Ca^{2+}, leading to the opening of the SK channel pore. This hypothesis is consistent with previous NMR studies on EF-hand proteins suggesting that substitution of lanthanide ions for Ca^{2+} does not significantly alter the conformation of the proteins (reviewed in ref. 22).

Ligand Binding at the N-lobe of CaM Gates SK Channels. Interestingly, previous biochemical studies showed that lanthanide ions bind to the two lobes of free CaM with very different affinities. Whereas lanthanide ions bind to the N-lobe of CaM with nanomolar affinity, they bind to the C-lobe of CaM with only slightly higher affinity than Ca^{2+}, with K_d in the μM range (19, 21). In contrast, Ca^{2+} binds to the C-lobe of CaM with slightly higher affinity than to the N-lobe, but all four binding sites in both C- and N-lobe of CaM have K_d for Ca^{2+} in the μM range (23, 24). In light of this distinction, the high apparent affinity for the activation of SK channel by lanthanide ions has important implications on the gating mechanism. The nanomolar apparent affinity measured in this study suggests that lanthanide ions specifically bind to the N-lobe of CaM to activate SK channels, because at nanomolar concentration range, binding at the C-lobe does not occur.

Structural and functional studies on SK channels have suggested that the N-lobe of associated CaM is solely responsible for ligand binding (3, 4). However, in light of some experimental limitations in these studies (see Introduction), it is important to verify this proposed molecular mechanism in a more intact and complete system. In our study, SK channels are functionally associated with endogenous wild-type CaM. Although our results do not directly indicate whether the C-lobe of CaM associated with SK channels can still bind ligands, it is clear that ligand binding at the N-lobe of CaM is sufficient to fully open the channels.

Our kinetic measurements of SK channel deactivation also indicate that ligand binding at the N-lobe of CaM is responsible for channel gating. Previous biochemical experiments with purified CaM and its tryptic fragments containing individual lobes showed that Tb^{3+} dissociates from the N-lobe of CaM with time constants of a few seconds. This rate is significantly slower than the dissociation rate of Tb^{3+} from the C-lobe of CaM ($\tau \approx 0.1$–1 s), and much slower than the dissociation rate of Ca^{2+} from either lobe of CaM ($\tau \approx 4$–40 ms) (17, 18). Our data show that when SK channels are activated purely by saturating concentration of Tb^{3+}, the deactivation process has a time constant of approximately 10 s. The closing of SK channels during deactivation does not provide a direct measurement of the dissociation rate of Tb^{3+}. However, by comparison with the fast deactivation in the case of Ca^{2+}, it is evident that dissociation of Tb^{3+} from CaM associated with SK channels has time constants on the order of a few seconds. The time course of the slow deactivation is in excellent agreement with the biochemically measured dissociation rate of Tb^{3+} from the N-lobe of CaM, but slower than would be expected for the dissociation rate from the C-lobe (18).

The above discussion was based on the assumption that lanthanide-binding properties of the two lobes of CaM (if they can still bind ligand) are not dramatically altered by the interaction with SK channels. Although cases exist where ligand binding of CaM is affected by interaction with its effector proteins (24, 25), it is unlikely that the C-lobe of CaM will be modified by the interaction with SK channel such that it mimics both the affinity and kinetic properties of the N-lobe for lanthanide binding. In light of the previous structural and mutational studies on SK channels (3, 4), and the biochemical findings that individual N and C-lobes of CaM in tryptic fragments maintain their affinity and kinetics for ligand binding as in intact protein (17, 18, 23), it is reasonable to conclude that the activation of SK channels by lanthanide ions is the result of binding to the N-lobe of CaM, which preserves its lanthanide binding properties when CaM is associated with SK channels.

Lanthanide ions have been instrumental in understanding the mechanisms of Ca^{2+}-binding proteins including CaM. Our finding that lanthanide ions can fully activate SK channels by binding to the Ca^{2+}-binding sites in CaM promises new approaches to study the gating mechanisms of SK channels. Related ligands with distinctive functional effects have become powerful tools in elucidating the gating mechanisms of ligand-gated ion channels such as glutamate receptor channels (reviewed in ref. 26). Lanthanide ions may prove to be the equivalent tools for the study of SK channels. Furthermore, the unique spectroscopic features of lanthanide ions in combination with electrophysiological recordings will likely provide very useful approaches to directly correlate ligand binding to channel opening in the functionally complete SK channel complex.

Materials and Methods

Channel Expression. All experiments were performed on the rSK2 clone of the SK channel kindly provided by the Adelman lab (Vollum Institute, Oregon Health and Science University). The clone was introduced into the pOX vector, from which cRNA was transcribed *in vivo*. Approximately 10–30 ng of rSK2 cRNA was injected into *Xenopus laevis* oocytes 2–6 days before recording.

Electrophysiology. All recordings were performed in the inside-out patch clamp configuration as described in ref. 27. Data were sampled at 20-μs intervals after low-pass filtering at 5 KHz using the built-in filter of the amplifier. For long recordings data were sampled at 100-μs intervals. No correction was made for the small (<5 mV) voltage errors because of junction potential and series resistance. All experiments were performed at 22 °C. Data analysis, curve fitting and plotting were performed with *IGOR Pro* software (WaveMetrics). Average results are presented as mean ± SD.

Solutions. The extracellular (pipette) solution contained (in mM): 140 $KMeSO_3$, 5 Hepes, 2 KCl, and 2 $MgCl_2$, pH 7.20. The base internal (bath) solution (BIS) contained: 136 $KMeSO_3$, 5 Hepes, and 6 KCl, pH 7.20. For solutions containing Ca^{2+} chelators, 5 mM chelator (HEDTA for $[Ca^{2+}]$ of 0.77 μM and above, EGTA for 0.55 μM and below) was added to the BIS. To achieve the desired free $[Ca^{2+}]$, $CaCl_2$ was added based on calculations using the WEBMAXC program (Stanford University). The actual free $[Ca^{2+}]$ in the final solutions was determined by measurements with a Ca^{2+}-sensitive electrode (Orion Research, Inc.). Solution with 5 mM EGTA and no added Ca^{2+} was considered Ca^{2+} free.

All experiments with Tb^{3+} and some with Ca^{2+} were conducted using chelator-free solution (CFS). Great care was taken in the preparation of this solution to reduce contamination by Ca^{2+} or Ca^{2+} chelators. All surfaces in contact with CFS were washed thoroughly with purified water from a Nanopure water system (Barnstead International). To remove contaminating Ca^{2+}, BIS was passed through columns made of Chelex 100 resin (Bio-Rad). The columns were prepared and used according to the manufacturer's instructions. Before use the column (≈15 g of resin) was first washed with 500 ml of water, then with BIS until the pH of the effluent stabilized at 7.2. Solution was passed through a column at least 10 times, then passed through a second column repeatedly until the contaminating Ca^{2+} level reached a minimum (see below).

The contaminating Ca^{2+} concentration in the final solution was measured with a Ca^{2+}-sensitive dye, Fura-2 (Invitrogen), using a spectrophotometer (Beckman). The absorption spectra of Fura-2 in the Ca^{2+}-free form (CFS + 2 μM Fura-2 + 1 mM EGTA) and in the Ca^{2+}-loaded form (CFS + 2 μM Fura-2 + 200 μM $CaCl_2$) were used to linearly fit the absorption spectrum of Fura-2 in CFS to estimate contaminating Ca^{2+} levels. With enough passes through the columns, we were able to routinely reduce the contaminating Ca^{2+} levels to approximately 300 nM, whereas more passes did not lead to further reduction. Different batches of CFS used in this study had contaminating Ca^{2+} levels

within ± 100 nM of 300 nM. CFS was filtered with 0.02-μm syringe filters (Anotop 25, Whatman International Ltd.) immediately before use to remove possible free resin particles. Open probability of SK channels in CFS was usually so low that only single-channel openings were visible. In some experiments the baseline current levels in CFS were considered as leak for correction. In other cases where they were available, current levels in Ca^{2+}-free solution (5 mM EGTA) were used for leak correction. Leak corrections (usually 5–20 pA at −80 mV) had little effect on the fits of dose-response relationships.

Recording Conditions. For most experiments, desired amounts of Tb^{3+} ($TbCl_3$) or Ca^{2+} ($CaCl_2$) were added directly to CFS by using stock solutions. $CaCl_2$ stock (0.1 mM and 1 mM) in CFS was prepared from the 0.1 M calcium standard (Orion). 10 mM $TbCl_3$ was prepared in CFS at pH 2 with added $HMeSO_3$, from which 1 μM $TbCl_3$ stock in CFS was prepared by serial dilutions immediately before use. Because of the low final concentrations used, adding $TbCl_3$ did not result in changes of pH in the bath solution. Tb^{3+} was found to be difficult to wash off from all surfaces in contact. Because of this limitation, all Tb^{3+} dose-response relationships were only measured with increasing concentrations. To avoid contamination between experiments, in many cases a freshly washed disposable Petri dish was used as the recording chamber for each experiment. In other cases where dose-response relationships were measured under two different conditions, a reusable perfusion chamber was used. In these experiments, CFS with increasing amounts of added Ca^{2+} or Tb^{3+} were first applied to the patch, followed by chelator-containing solutions with different free Ca^{2+} concentrations. Solution of >10 times the volume of the recording chamber was washed through to achieve a complete solution change. This chamber was extensively washed after each experiment to remove residual Tb^{3+} or Ca^{2+} chelator. Additionally, oocytes were washed three times with purified water before being transferred to the recording chamber to avoid carrying over Ca^{2+} or chelators.

In experiments to measure the deactivation of SK channels, a syringe connected to a quartz sewer pipe (100 μm in diameter) was used to deliver Ca^{2+}-free solution (5 mM EGTA). After the SK current stabilized, the recording pipette was manually moved into a laminar flow of Ca^{2+}-free solution from the sewer pipe during continuous recording of current. By using an open electrode, we estimated that it routinely requires only a few ms to move the electrode across the solution interface, judged by the current changes because of junction potential difference. Complete solution change around an inside-out patch takes longer time (a few tens of ms, as judged by changes in SK current when moving a patch into solutions with different K^+ concentrations). However, only a small fraction of 5 mM EGTA on the inside of the patch is necessary to effectively prevent ligand rebinding during deactivation. This should require much less time to achieve than a complete solution change. It is likely that our measured deactivation time constants are not significantly affected by the solution change, although a slight overestimate is expected in the fast time constants for the deactivation of SK channels activated by Ca^{2+}.

ACKNOWLEDGMENTS. The authors wish to thank Dr. Adron Harris's lab (University of Texas at Austin) for generously providing the *Xenopus* oocytes for this study. We thank Dr. Thomas Middendorf for his continuous support and advice throughout this project and for his comments on the manuscript. We are also thankful to Drs. Gary Yellen, Jenni Greeson, Brent Halling and Riina Luik for critically reading the manuscript.

1. Xia XM, *et al.* (1998) Mechanism of calcium gating in small-conductance calcium-activated potassium channels. *Nature* 395:503–507.
2. Maylie J, Bond CT, Herson PS, Lee WS, Adelman JP (2004) Small conductance Ca^{2+}-activated K^+ channels and calmodulin. *J Physiol* 554:255–261.
3. Schumacher MA, Rivard AF, Bachinger HP, Adelman JP (2001) Structure of the gating domain of a Ca^{2+}-activated K^+ channel complexed with Ca^{2+}/calmodulin. *Nature* 410:1120–1124.
4. Keen JE, *et al.* (1999) Domains responsible for constitutive and Ca^{2+}-dependent interactions between calmodulin and small conductance Ca^{2+}-activated potassium channels. *J Neurosci* 19:8830–8838.
5. Soh H, Park CS (2001) Inwardly rectifying current-voltage relationship of small-conductance Ca^{2+}-activated K^+ channels rendered by intracellular divalent cation blockade. *Biophys J* 80:2207–2215.
6. Kilhoffer MC, Demaille JG, Gerard D (1980) Terbium as luminescent probe of calmodulin calcium-binding sites; domains I and II contain the high-affinity sites. *FEBS Lett* 116:269–272.
7. Kilhoffer MC, Gerard D, Demaille JG (1980) Terbium binding to octopus calmodulin provides the complete sequence of ion binding. *FEBS Lett* 120:99–103.
8. Mulqueen P, Tingey JM, Horrocks WD, Jr. (1985) Characterization of lanthanide (III) ion binding to calmodulin using luminescence spectroscopy. *Biochemistry* 24:6639–6645.
9. Wang CL, Leavis PC, Gergely J (1984) Kinetic studies show that Ca^{2+} and Tb^{3+} have different binding preferences toward the four Ca^{2+}-binding sites of calmodulin. *Biochemistry* 23:6410–6415.
10. Wang CL, Aquaron RR, Leavis PC, Gergely J (1982) Metal-binding properties of calmodulin. *Eur J Biochem* 124:7–12.
11. Wallace RW, Tallant EA, Dockter ME, Cheung WY (1982) Calcium binding domains of calmodulin. Sequence of fill as determined with terbium luminescence. *J Biol Chem* 257:1845–1854.
12. Sotiroudis TG (1986) Lanthanide ions and Cd^{2+} are able to substitute for Ca^{2+} in regulating phosphorylase kinase. *Biochem Int* 13:59–64.
13. Bentrop D, *et al.* (1997) Solution structure of the paramagnetic complex of the N-terminal domain of calmodulin with two Ce^{3+} ions by ^{1}H NMR. *Biochemistry* 36:11605–11618.
14. Moeller T, *et al.* (1965) The coordination chemistry of yttrim and the rare earth metal ions. *Chem Rev* 65:1–50.
15. Lee WS, Ngo-Anh TJ, Bruening-Wright A, Maylie J, Adelman JP (2003) Small conductance Ca^{2+}-activated K^+ channels and calmodulin: Cell surface expression and gating. *J Biol Chem* 278:25940–25946.
16. Bildl W, *et al.* (2004) Protein kinase CK2 is coassembled with small conductance Ca^{2+}-activated K^+ channels and regulates channel gating. *Neuron* 43:847–858.
17. Martin SR, Andersson Teleman A, Bayley PM, Drakenberg T, Forsen S (1985) Kinetics of calcium dissociation from calmodulin and its tryptic fragments. A stopped-flow fluorescence study using Quin 2 reveals a two-domain structure. *Eur J Biochem* 151:543–550.
18. Martin SR, Linse S, Bayley PM, Forsen S (1986) Kinetics of cadmium and terbium dissociation from calmodulin and its tryptic fragments. *Eur J Biochem* 161:595–601.
19. Bruno J, Horrocks WD, Jr., Zauhar RJ (1992) Europium(III) luminescence and tyrosine to terbium(III) energy-transfer studies of invertebrate (octopus) calmodulin. *Biochemistry* 31:7016–7026.
20. Hirschberg B, Maylie J, Adelman JP, Marrion NV (1998) Gating of recombinant small-conductance Ca-activated K^+ channels by calcium. *J Gen Physiol* 111:565–581.
21. Horrocks WD, Jr., Tingey JM (1988) Time-resolved europium(III) luminescence excitation spectroscopy: Characterization of calcium-binding sites of calmodulin. *Biochemistry* 27:413–419.
22. Capozzi F, Casadei F, Luchinat C (2006) EF-hand protein dynamics and evolution of calcium signal transduction: An NMR view. *J Biol Inorg Chem* 11:949–962.
23. Minowa O, Yagi K (1984) Calcium binding to tryptic fragments of calmodulin. *J Biochem* 96:1175–1182.
24. Johnson JD, Snyder C, Walsh M, Flynn M (1996) Effects of myosin light chain kinase and peptides on Ca^{2+} exchange with the N- and C-terminal Ca^{2+} binding sites of calmodulin. *J Biol Chem* 271:761–767.
25. Yazawa M, Vorherr T, James P, Carafoli E, Yagi K (1992) Binding of calcium by calmodulin: Influence of the calmodulin binding domain of the plasma membrane calcium pump. *Biochemistry* 31:3171–3176.
26. Mayer ML (2005) Glutamate receptor ion channels. *Curr Opin Neurobiol* 15:282–288.
27. Li W, Aldrich RW (2006) State-dependent block of BK channels by synthesized shaker ball peptides. *J Gen Physiol* 128:423–441.